Surface-phonon dispersion of a NiO(100) thin film

K. L. Kostov,[1,2] S. Polzin,[1] S. K. Saha,[3] O. Brovko,[3] V. Stepanyuk,[3] and W. Widdra[1,3,*]
[1]*Institute of Physics, Martin-Luther-Universität Halle-Wittenberg, 06120 Halle, Germany*
[2]*Institute of General and Inorganic Chemistry, Bulgarian Academy of Sciences, 1113 Sofia, Bulgaria*
[3]*Max Planck Institute of Microstructure Physics, 06120 Halle, Germany*
(Received 13 April 2013; revised manuscript received 28 May 2013; published 17 June 2013)

A well-ordered 25 ML epitaxial NiO(100) film on Ag(100) as prepared by layer-by-layer growth has been characterized by high-resolution electron energy loss spectroscopy. Six different phonon branches have been identified in the $\overline{\Gamma}\,\overline{\mathrm{X}}$ direction of the surface Brillouin zone and are compared with first-principles phonon calculations. Whereas the surface Rayleigh mode shows a strong upward dispersion of 173 cm^{-1} in agreement with observations for the NiO(100) single crystal, the other surface phonons and surface resonances show only smaller dispersion widths in $\overline{\Gamma}\,\overline{\mathrm{X}}$ direction. The Wallis and the Lucas phonons are localized at 425 and 367 cm^{-1} at the $\overline{\Gamma}$ point, respectively. Additionally, two phonons are identified that have stronger weight at the zone boundary at 194 and 285 cm^{-1} and that become surface resonances at the zone center. The dominant spectral feature is the Fuchs-Kliewer (FK) phonon polariton at 559 cm^{-1}, which is excited by dipole scattering and exhibits a rather broad non-Lorentzian lineshape. The lineshape is explained by a FK splitting resulting from the splitting of bulk optical phonons due to antiferromagnetic order. This view is supported by calculations of the surface-loss function from bulk reflectivity data.

DOI: 10.1103/PhysRevB.87.235416 PACS number(s): 68.35.Ja, 68.47.Gh, 68.49.Jk

I. INTRODUCTION

The late transition metal monoxides have been experimentally studied as prototypes of strongly correlated electron systems that exhibit a magnetic, mainly antiferromagnetic, spin order. The strong electron-electron correlations within the *d* transition metal electrons lead to the formation of either Mott-Hubbard or charge-transfer insulators despite the presence of partially filled *d* band. Among all transition metal monoxides, NiO can be considered as the benchmark charge-transfer insulator with a band gap of about 4.0 eV. Therefore, it has been studied in detail with respect to its electronic and optical properties.[1–3] The phonon properties of bulk NiO have been studied since the mid-1970s and have recently attracted further attention due to their spin-phonon coupling.[4–9] The surface-phonon dispersion has been studied for the low-index (100) cleavage plane by high-resolution electron energy loss spectroscopy (HREELS) and inelastic Helium atom scattering (HAS) previously.[10–12] However, charging of the NiO single crystal restricted previous electron scattering investigations in the accessible energy range and prevented full dispersion analysis.[10] The high-resolution HAS studies, on the other hand, have been limited to the investigation of the very low-lying excitations.[12] In the present study, we use HREELS on a 5-nm-thick NiO(100)-(1 × 1) film epitaxially grown on a metallic Ag(100) where the NiO(100) film is structurally equivalent to a NiO(100) single crystal but avoids significant charging.

In HREELS, the surface phonons are excited by dipole or by electron impact scattering depending on the specular (no electron momentum transfer parallel to the surface) or on the off-specular scattering geometry, respectively. The selection rules for specular scattering are identical as for infrared absorption spectroscopy. The specular HREEL spectra of NiO(100) are dominated by the macroscopic Fuchs-Kliewer (FK) phonon polariton[13,14] at 69.5 meV (560.5 cm^{-1}), as reported in the early work of Cox and Williams.[15] A slightly higher frequency of 70.5 meV (564 cm^{-1}) has been reported in a later study where multiple FK phonon excitations have been analyzed.[16,17] In a combined experimental and theoretical approach, Oshima has studied the surface-phonon dispersions along the $\overline{\Gamma}\,\overline{\mathrm{X}}$ direction of the surface Brillouin zone (SBZ) by HREELS.[10] Besides the intense FK phonon at 67.4 meV (543.6 cm^{-1}) at $\overline{\Gamma}$, three additional phonon modes have been detected and assigned to Rayleigh (S_1), Wallis (S_2), and Lucas (S_4) phonons. The principal surface-phonon dispersions have been compared with slab calculations using the shell model with parameters identical to the corresponding bulk values.[10] The optical Wallis and Lucas phonons appear as gap modes corresponding to vibrations perpendicular and parallel to the surface, respectively.[18,19] According to the calculations of Oshima, the Wallis (S_2) mode is located in the gap of the optical band around the $\overline{\Gamma}$ point, whereas the Lucas (S_4) mode is found between the projected acoustic and optical bulk bands.[10] A later high-resolution HAS study determined the dispersion of the low-energy Rayleigh mode (RW, S_1) and identified a surface phonon (S_6) in the acoustic bulk gap near the $\overline{\mathrm{X}}$ point [5, 6].[12,20] However, as the authors noted, the observation of the latter mode is not compatible with the shell model calculations[10] using the bulk values of the force constants also for the surface region.

II. EXPERIMENTAL DETAILS

The measurements have been performed in a two-chamber ultra-high vacuum (UHV) apparatus with a base pressure of about 3×10^{-9} Pa, as described in detail elsewhere.[21,22] In the preparation chamber that is equipped with X-ray photoelectron spectroscopy (XPS), low-energy electron diffraction (LEED) optics, and temperature-programmed desorption facilities, the cleaning of the Ag(100) sample has been carried out by standard procedure that includes repeated cycles of Ar^+ sputtering (3 μA at 1 keV ion energy) and subsequent annealing at 700 K. The second chamber houses an HREEL spectrometer (Delta 05, Specs GmbH, Berlin) with a total energy resolution of

about 1 meV (~8 cm^{-1}) and corresponding specular count rates of 10^6 s^{-1} at 4 eV for bare and adsorbate covered metal surfaces.[22–24] In the present study, the phonon dispersions have been measured in off-specular geometry along the [011] direction, which corresponds to $\overline{\Gamma X}$ in the SBZ. The scattering geometry allows variation of the electron incidence as well as the emission angle. If not stated otherwise, a total reflection angle of 120° is used, and both incidence and emission angle are varied simultaneously as in previous studies.[21,25]

The NiO(100) film with a thickness of approximately 25 ML has been prepared by layer-by-layer growth upon Ni evaporation in an oxygen pressure of 2×10^{-7} mbar at 300 K.[26,27] The deposition rate was 0.5 ML/min. The oxygen inlet has been realized via directional dosing ensuring an partial oxygen pressure at least one order of magnitude higher at the Ag(100) sample. Additionally, the NiO(100) films have been annealed at 550 K in the same oxygen atmosphere. The improvement of the ordering was monitored by HREELS and LEED. The NiO(100) thickness calibration has been realized a posteriori by observation of *in situ* growth oscillations during the beginning of the NiO growth using specular medium-energy electron reflection similar as for reflection high-energy electron diffraction (RHEED) with a relative accuracy of the thickness of 10%.

III. RESULTS AND DISCUSSION

A. Ordering of the NiO layer

For a 25-ML NiO(100) thin film on Ag(100), which has been grown as described above, the strong (1×1) LEED pattern is shown in the inset of Fig. 1. At this coverage, the film is already relaxed to the NiO bulk in plane lattice constant. The absence of additional LEED spots from a Moiré pattern or a mosaic superstructure due to the lattice mismatch of 2% with respect to Ag(100) ensures that electron back diffraction stems solely from the NiO thin film. Note that in the 10 to 20 ML range, we do observe mosaic and Moiré superstructure patterns in sequence as consequence of misfit dislocations and lattice mismatch. In comparison, the HREELS elastic-peak intensity between the centers (in $\overline{\Gamma}\,\overline{X}\,\overline{\Gamma'}$ direction) of the first and second SBZs is shown in Fig. 1 for the 25-ML film. Using an electron energy of 144 eV, the elastic-peak intensity at the next $\overline{\Gamma'}$ point is approximately five times lower compared to the intensity at the center of the first SBZ. This corresponds well to the ratio between the first- and second-order spot intensities observed in LEED with similar electron energy (inset of Fig. 1).

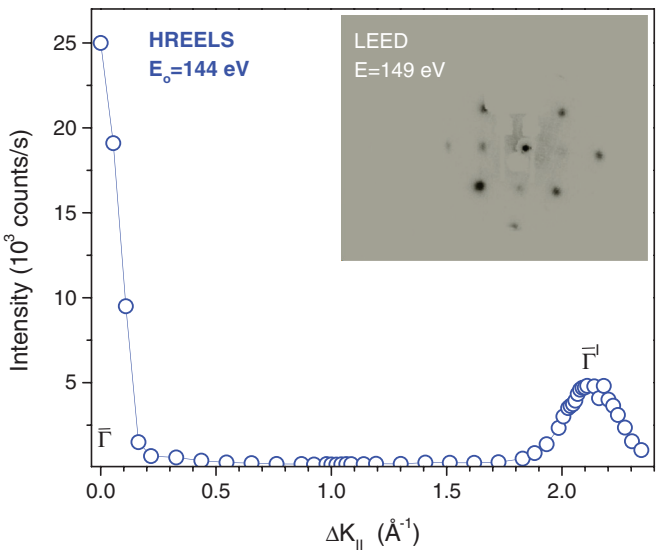

FIG. 1. (Color online) Elastic-peak intensity as function of momentum transfer $\Delta k_{\|}$ along the $\overline{\Gamma}\,\overline{X}\,\overline{\Gamma'}$ direction. The energy of the scattered electron is 144 eV. The LEED pattern of NiO(100) for an electron energy of 149 eV is shown in the inset.

B. Vibrational measurements at the $\overline{\Gamma}$ point

For NiO(100) thin films of 25 ML, the most intense loss in the specular HREEL spectrum corresponds to the excitation of the FK phonon polariton with an energy of $\hbar\omega = 559.0$ cm^{-1} (69.3 meV). Figure 2 presents the loss and energy gain regions for a well-ordered 25-ML NiO(100)-(1×1) film where the dominant features originate from multiple FK phonon excitations and FK annihilation. As has been demonstrated for many oxide surfaces, the FK frequency and the spectral shape of the energy loss in specular scattering geometry is completely governed by the surface dielectric response.[28,29] Here the energy of the FK phonon is directly related to the frequencies of the bulk transverse optical (TO) and the longitudinal optical (LO) phonons via

$$\hbar\omega = [(\varepsilon_o + 1)/(\varepsilon_\infty + 1)]^{1/2}\hbar\omega_{TO}, \qquad (1)$$

where ε_o and ε_∞ are the static and high-frequency dielectric constants, respectively. Based on the Lyddane-Sachs-Teller relation, ε_0 is directly related to ω_{TO}, ω_{LO}, and ε_∞. Based on the NiO bulk properties[7] of $\varepsilon_o = 11.9$, $\varepsilon_\infty = 5.25$, and

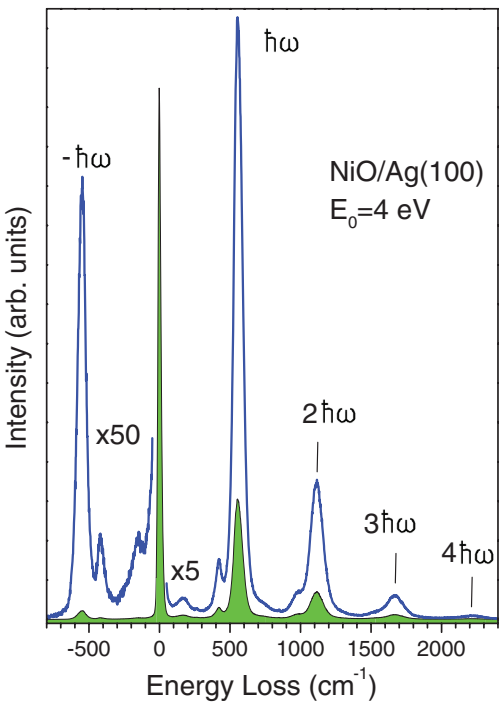

FIG. 2. (Color online) High-resolution electron energy loss spectrum for a 25-ML-thick NiO(100) layer on Ag(100) in specular scattering geometry for an electron energy of 4 eV.

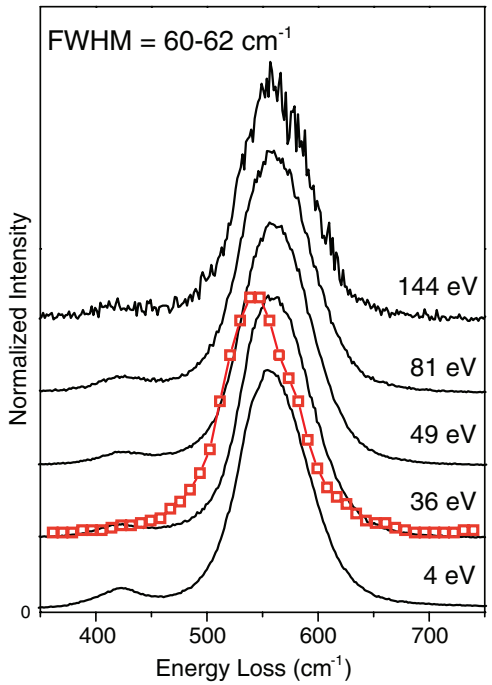

FIG. 3. (Color online) HREEL spectra of the FK phonon region for a 25-ML-thick NiO(100) layer on Ag(100) for five different primary electron energies as indicated. The data by Oshima (Ref. 10) for a NiO(100) single crystal and a primary energy of 41 eV are shown as open squares for comparison.

$\omega_{TO} = 388$ cm^{-1}, we expect the surface FK phonon in the observed spectral range as discussed in full detail in the following and as reported previously for NiO films and single crystals.[15,30] It is important to note that the spectral shape in the region of the FK phonon is independent on the electron kinetic energy since it is determined by the surface-loss function. This is shown in Fig. 3 for five different electron energies. The experimental energy resolution, here about 22–28 cm^{-1}, is well below the full width at half maximum (FWHM) of the phonon peak, which amounts to 60–62 cm^{-1} for all data sets in the kinetic energy range from 4 to 196 eV. Moreover, the same FWHM for the FK phonon has been measured by Oshima at 41 eV on a single crystal, as marked by red open squares in Fig. 3 for comparison.[10] Therefore, the surface-loss function can be evaluated from the data and compared with high-resolution optical data for a NiO(100) single crystal.[9] Note that the small shift between the data of Oshima and the data presented here is fully accounted for by the dielectric response at finite thickness for the 25-ML NiO(100) film. This thickness dependence has been evaluated previously for NiO as well as MnO on different substrates.[31,32]

Besides the FK phonon peak, the HREEL spectrum in Fig. 2 shows strong losses at 421.2 cm^{-1} and 170.3 cm^{-1}, which are clearly visible also on the energy-gain side. While the first peak is attributed to the NiO Wallis mode, the nature of the latter lower-frequency loss is less clear and will be assigned to a phonon-resonance feature. In the following discussion of the spectra, at the $\overline{\Gamma}$ point we identify additional phonons at 266.6 and 362 cm^{-1}. Both, as well as the loss at 170.3 cm^{-1}, are identified for the first time.

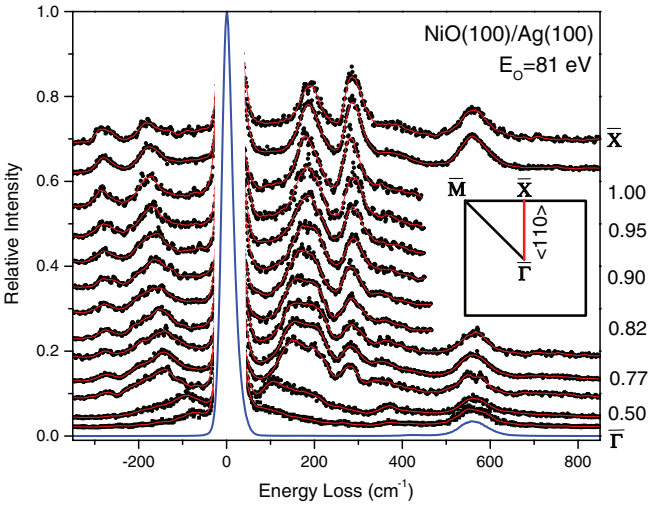

FIG. 4. (Color online) Off-specular HREEL spectra for a 25 ML NiO(100) layer on Ag(100) measured with an electron energy of 81 eV along the $\overline{\Gamma}\,\overline{X}$ direction. From bottom to top the off-specular angle is increased successively from 0 (bottom spectrum) by 3° for each spectrum. The corresponding momentum transfer (in Å^{-1}) is labeled on the right side of the figure for every second spectrum. The structure of the first Brillouin zone in reciprocal space is shown in the inset.

C. Experimental identification of different phonon modes

To allow for a full phonon-dispersion mapping up to the SBZ boundary, a wide range of kinetic energies from 4 to 196 eV has been used as demonstrated in Fig. 4 for scattering along the high-symmetry $\overline{\Gamma}\,\overline{X}$ direction. The SBZ with the high-symmetry points is indicated in the inset. Besides the FK phonon at about 559 cm^{-1}, four additional low-frequency modes can be identified, namely the Rayleigh phonon with a strong dispersion between 0–175 cm^{-1} and modes at ~180, ~270, and ~370 cm^{-1}. The later modes show small dispersions, and their nature will be discussed below based on a comparison with bulk phonon calculations. The intensity of the loss at ~270 cm^{-1} is weakest at low parallel momentum values, but the feature becomes dominant in the off-specular spectrum at high $\Delta k_{\parallel}$ near the SBZ boundary at the $\overline{X}$ point (Fig. 4). The change of its inelastic cross section with momentum may be interpreted as due to a different polarization of the mode at low and high wave vectors. As discussed later, the mode might change its character at high $\Delta k_{\parallel}$ toward a more decoupled surface phonon.

In general, the inelastic excitation cross sections also depend strongly on incident electron energy.[21,33] Due to this electron energy dependence, it is possible to resolve different phonon modes by comparing the off-specular spectra obtained by different electron energies at a fixed momentum transfer. This is demonstrated in Fig. 5 where HREEL spectra are compared for *different* energies but for a *fixed* $\Delta k_{\parallel} = 0.76$ Å^{-1}. All four spectra in Fig. 5 should show the same phonon modes, and only the excitation cross sections might vary between the measurements. Therefore, all spectra have to be fitted consistently by the same set of phonon frequencies. This allows identifying six different phonon modes in Fig. 5. The spectrum taken at 144 eV clearly shows the presence of phonons at 139 and 210 cm^{-1}. Whereas the former is also well confirmed at

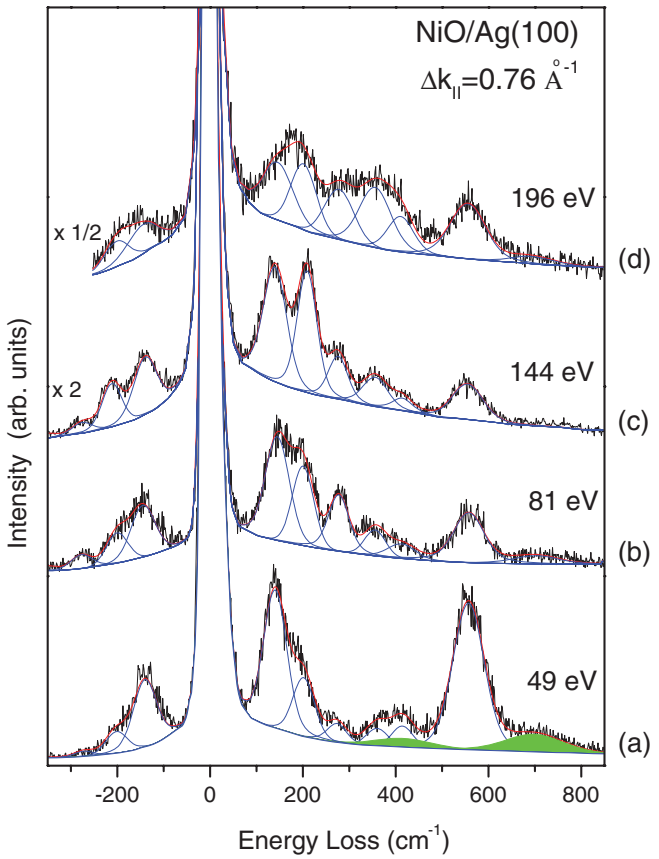

FIG. 5. (Color online) Off-specular HREEL spectra at constant momentum transfer $\Delta k_{\parallel} = 0.76$ Å^{-1} but for different electron energies (indicated in the figure). The contribution of the different phonon modes and their sum are shown with blue and red curves, respectively. In the bottom spectrum (a) the gain- and loss-RW peaks around the FK phonon peak are colored in green.

49 eV, the latter is only present as shoulder there (Fig. 5). These two phonon modes are visible on the energy loss as well as on the energy gain side of the spectra with intensities that strictly obey the relation

$$I_{\text{gain}}/I_{\text{loss}} = \exp(-\hbar\omega/kT), \tag{2}$$

where $T = 300$ K, as experiments have been performed at room temperature. This cross-section relation for phonon excitation and annihilation in HREELS has been used as strict constraint in the evaluation of the data. The spectrum with electron energy of 81 eV provides clear evidence for the phonon excitation at 278 cm^{-1} (Fig. 5). With this input and the clear observation of a phonon at 354 cm^{-1} in the 144 eV spectrum, in all four spectra the broad loss structure centered at about 340 cm^{-1} can be decomposed into three separate contributions located at 278, 354, and 410 cm^{-1}.

The strongly dipole-active FK phonon is visible at all scattering conditions for electron energies between 4 and 196 eV. Its intensity is stronger in off-specular measurements at lower electron energies (4–49 eV), whereas at higher energies (81–196 eV), it is comparable to or lower as the lower-frequency losses (Fig. 5). Its intensity drops strongly with off-specular angle, and the remaining loss intensities at 559 cm^{-1} in all off-specular data are interpreted as excitations of the FK phonon at $k_{\parallel} = 0$ with additional (not momentum conserving) scattering at defects. Additionally, the excitation of combination losses between the strong FK phonon and other phonon modes has been observed. In fact, in the lowest spectrum in Fig. 5, the weak peak at 700 cm^{-1} (colored in green) can be identified as combination of the FK phonon at about 559 cm^{-1} (with $k_{\parallel} = 0$) and the RW phonon at 139 cm^{-1} with $k_{\parallel} = 0.76$ Å^{-1}. Note that also a combination with a RW gain peak at 420 cm^{-1} is compatible with experimental data. The phonon peaks in Fig. 5 at 139, 210, and 275 cm^{-1} show line widths of 40 to 50 cm^{-1}, which are all significantly broader than the experimental resolution used here and as extracted from the width of the zero loss peak (22–28 cm^{-1} in the different spectra of Fig. 5). This additional phonon broadening might correspond to a finite phonon lifetime or a fast phonon dephasing.

D. Surface phonons at $\overline{\text{X}}$ point

At the SBZ boundary at the $\overline{\text{X}}$ point, we observe six phonon-induced losses, as displayed in Fig. 6. The most intense features are attributed to the excitations of FK and Rayleigh phonons at ~558 cm^{-1} and 173.3 cm^{-1}, respectively. The figure demonstrates that the FK phonon intensity has an inverse dependence on the electron kinetic energy, and at low energies it dominates in the loss spectra. On the other hand, the Rayleigh phonon together with the newly detected phonons at 194, 350, and 408 cm^{-1} dominate at higher electron energies.

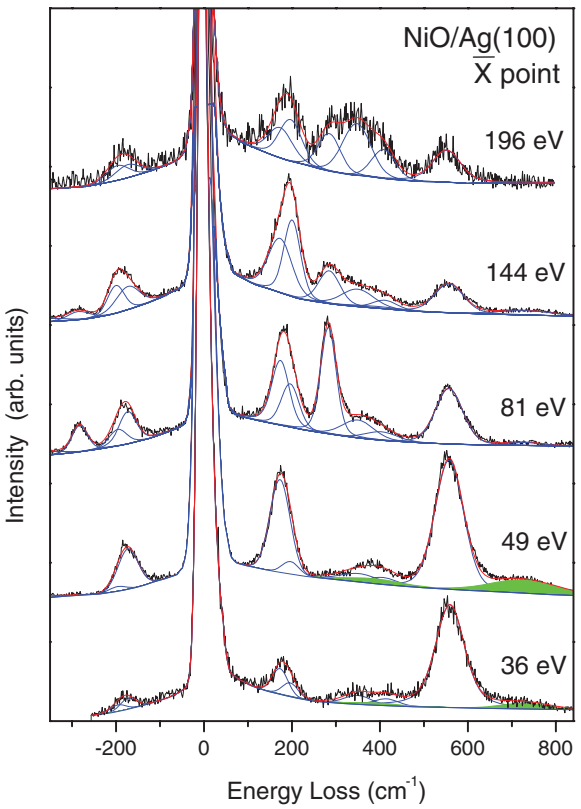

FIG. 6. (Color online) Off-specular HREEL spectra at the $\overline{\text{X}}$ point measured with different electron energies as indicated. The contributions of the different phonon modes obtaining from the fitting procedure and their sum are shown with blue and red curves, respectively.

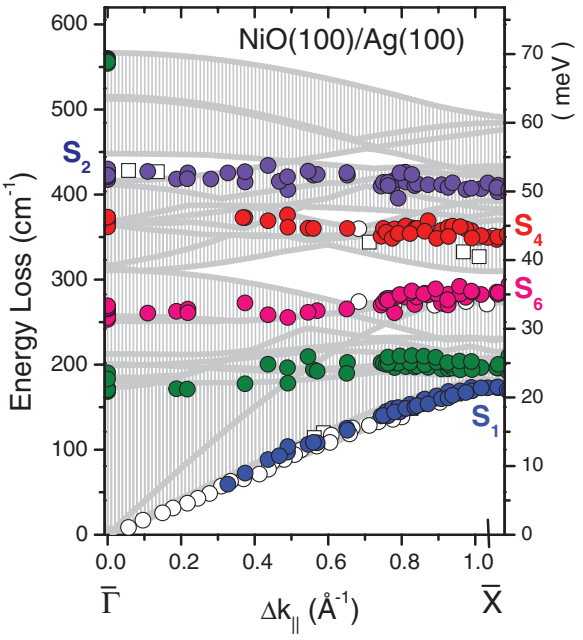

FIG. 7. (Color online) Experimental phonon dispersion (solid and open symbols) for the NiO(100) layer on Ag(100) along $\overline{\Gamma}\,\overline{X}$ direction at 300 K. Solid circles denote the present HREELS data whereas the open squares and circles mark previous HREELS (Ref. 10) and HAS (Ref. 12) results for a NiO(100) single crystal, respectively. The solid circles of a given color indicate one phonon branch. The hatched areas mark the surface-projected bulk phonon bands as derived from our DFT + U frozen phonon calculations.

Similar to the off-specular spectrum at $\Delta k_{\parallel} = 0.76$ Å^{-1} in Fig. 5, we observe again the broad loss due to the combined excitations of Rayleigh and FK phonons. These losses are colored in green in the spectra for low electron energies of 36 and 49 eV (Fig. 6). A significantly stronger intensity variation with electron energy is observed for the phonon at 285 cm^{-1}, which will be attributed to the S_6 gap mode between projected acoustic bulk bands (see also Fig. 7). Its maximum intensity is measured at an electron energy of 81 eV, whereas at 49 eV the excitation cross section vanishes.

E. Surface-phonon dispersion

In Fig. 7, the surface-phonon dispersion derived from a large data set of inelastic HREELS measurements along the high-symmetry $\overline{\Gamma}\,\overline{X}$ direction is shown together with the projected bulk phonon bands (hatched areas). The latter are derived from our frozen-phonon (PHONOPY) calculations using the DFT + U approach (QuantumEspresso) with an exchange-correlation functional of PBESOL (USPP) and an effective Hubbard U of 5.77 eV. It is worth mentioning that our frozen-phonon calculation for the bulk antiferromagnetic Type-II NiO, which uses an energy cutoff of 60 Ry and a $6 \times 6 \times 6$ k-mesh for the 32-atom $2 \times 2 \times 2$ supercell, can well reproduce the bulk phonon dispersion by Floris *et al.* calculated by density functional perturbation theory.[8]

In Fig. 7, the results from previous HREELS[10] and HAS[12,20] studies for a NiO(100) single crystal are also marked for comparison by open squares and circles, respectively. In general, our experimental data can be separated into six phonon branches. The lowest-frequency branch is attributed to the excitation of the RW phonon S_1, which is in very good agreement with the previous results of Oshima[10] and Witte *et al.* for NiO single crystals.[12,20] The latter studies reported for the RW frequency at the $\overline{X}$ point a value of 180 cm^{-1} (22.3 meV), whereas we measure a value of 173.3 ± 0.4 cm^{-1} (21.5 meV). The slightly higher frequency for this peak reported by the HAS study[12,20] might result from additional spectral weight from the next phonon branch, which is near the $\overline{X}$ point very close to the RW (Fig. 7, marked in green). The phonon branch directly above the RW starts from ∼175 cm^{-1} at the $\overline{\Gamma}$ point and reaches 194 cm^{-1} at the $\overline{X}$ point. This mode is reported for the first time here and can be seen as a strong and well-resolved peak in the second spectrum in Fig. 5 for an electron energy of 144 eV. It runs through a region of surface-projected bulk bands approximately following the flat-band edge of a bulk LA phonon band, which appears at the Γ point at 200 cm^{-1} due to the antiferromagnetic ordering. The newly observed surface mode therefore has the character of a surface resonance. A similar situation has been observed for CoO(100) near the $\overline{M}$ point where a phonon branch is predicted and described like an "optical" Rayleigh phonon S_1' because its frequency is very close to that of the RW.[12] This S_1' surface phonon at the $\overline{M}$ point represents a vibration of the oxygen ions whereas the Co ions are not moving.[12]

The third phonon branch, which begins at 266 cm^{-1} at $\overline{\Gamma}$, displays only a weak dispersion up to 285 cm^{-1} at the $\overline{X}$ point (Fig. 7). It has weaker intensity for smaller momenta, and only beyond $k_{\parallel} = 0.75$ Å^{-1} does it gain spectral weight. This can be seen directly in Fig. 4 for an electron energy of 81 eV. This behavior can be understood by looking at the projected bulk phonon bands in Fig. 7. Whereas initially this mode is only a weak surface resonance, it disperses in the projected bulk band gap at about 0.7 Å^{-1} and becomes a true surface phonon. At the $\overline{X}$ point, this phonon, labeled S_6, is dominating the spectrum at energy of 81 eV, as can be seen in Fig. 6 as well-resolved loss and gain peaks. This mode has been also detected by HAS for momentum transfer values higher than 0.65 Å^{-1}, in good agreement with our observations.[12] Note that our data indicate a well-developed surface-phonon character for this mode, which was under debate in the previous HAS study and which compares well with the case of CoO(100).[12]

The fourth phonon branch, which is marked as S_4 in Fig. 7, is identified as the Lucas mode in good agreement with previous HREELS and HAS [5,6] studies.[10,12,20] It exhibits a small dispersion between $\overline{\Gamma}$ and $\overline{X}$ from ∼367 to 350 cm^{-1}, respectively. In comparison to the bulk phonon data, one realizes that the Lucas mode that is typically located in the gap between the acoustic and optical bulk bands passes through the projected bulk density of states, which is marked as hatched area in Fig. 7. The related bulk modes are, however, the LA modes that are back-folded by the antiferromagnetic order, whereas in the nonmagnetic case in this spectral region, there is a bulk-phonon gap. Therefore, the low bulk density of states might explain why the Lucas mode still has spectral weight at the surface.

The phonon mode that starts from 425 cm^{-1} at the $\overline{\Gamma}$ point is experimentally observed throughout the SBZ and exhibits a small downward dispersion to 408 cm^{-1} at the $\overline{X}$ point. Therefore, it starts at $k_{\parallel} = 0$ above the flat bulk TO modes

at Γ and disperses slightly into the bulk bands at the $\overline{X}$ point based on the calculated bulk phonon dispersion. This mode is assigned to the Wallis (S_2) mode, in agreement with the modeling of Witte *et al.*[12] Initially it was observed for the NiO(100) single crystal by Oshima[10] in the vicinity of the $\overline{\Gamma}$ point, as marked by open squares in Fig. 7. However, our data (full symbols in Fig. 7) show a continuous dispersion of this branch up to the $\overline{X}$ point where the mode character switches to a surface resonance.

The highest-frequency FK mode at about 559 cm^{-1} is present in all spectra but does not show any peak shift with variation of the off-specular angle. As we discuss later in detail, this peak is dominantly excited by dipole scattering and therefore is determined by the FK frequency at $k_{\parallel} = 0$ in all spectra. Furthermore, this mode corresponds to the phonon polariton, which is a coupled surface excitation of the TO phonon with the electromagnetic field and is not considered in the phonon dispersion of Fig. 7. However, since its frequency for NiO is close to the bulk LO frequency at Γ, we can compare the experimental point for $\Delta k_{\parallel} = 0$ with the calculated bulk LO data in Fig. 7. The FK phonon agrees well with the top of the calculated bulk LO band at Γ, which underlines a correct theoretical description here.

Note that we find an additional weak loss feature, which shows a strong and initially linear dispersion between $\overline{\Gamma}$ and $\overline{X}$, as can be seen, e.g., in Fig. 5(a) at about 700 cm^{-1} for $\Delta k_{\parallel} = 0.76$ $Å^{-1}$. It is assigned to a combination band of the FK phonon and the acoustic Rayleigh phonon. This assignment explains fully the strong dispersion that runs parallel to the RW phonon.

F. Surface-phonon polariton

Within the dipolar-scattering mechanism and for sufficient thick layers, the intensities of dipolar losses with respect to the elastic peak are proportional to $E_0^{-1/2}$ (E_0 is the primary electron energy), whereas for ultrathin or adsorbate layers, this dependence is expected to be E_0^{-1} (see Ref. 34). Figure 8(a) shows the relative intensity of the FK phonon polariton in a double logarithmic plot as a function of the primary electron energy. A linear curve fitting to the experimental data results in a slope of −0.61. This value is close to the expected −0.5 for thick films, which indicates the dominant role of the dipolar-scattering mechanism in electron-FK phonon interaction and underlines a sufficient NiO layer thickness.

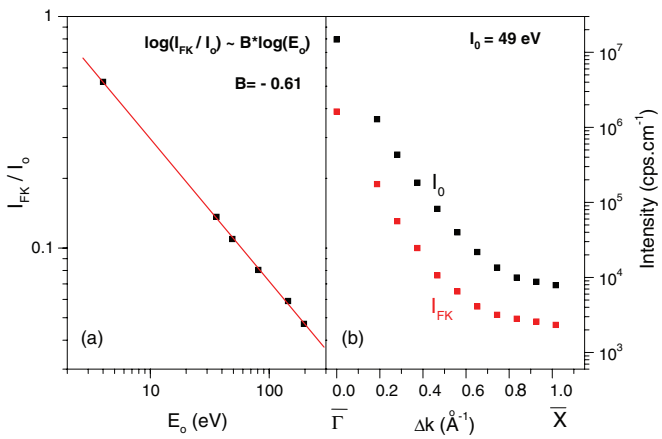

FIG. 8. (Color online) Relative intensity of the FK phonon as function of the electron kinetic energy in specular scattering geometry (a) and (b) as function of off-specular scattering angle for a fixed kinetic energy of 49 eV.

The dipolar excitation of the FK phonon is considered a small-angle scattering event; therefore, it should be visible in narrow momentum transfer region around the $\overline{\Gamma}$ point. On the other hand, in Figs. 5 and 6, the FK phonon peak is visible under all scattering conditions. Similarly, we note that the elastic peak is also visible under all scattering conditions and not only around the $\overline{\Gamma}$ point. For both, the zero-loss elastic and the FK phonon peak, the integrated intensities (peak areas) are shown in Fig. 8(b) as a function of parallel momentum for a primary energy of 49 eV. The intensities of both peaks decrease strongly with parallel momentum by more than three orders of magnitude. This behavior is expected for dipolar scattering with $\Delta k_{\parallel} = 0$, where the off-specular intensity is due to additional nonmomentum conserving scattering from surface defects. The approximately proportional decrease of both intensities is therefore a strong indication that the observed FK peaks along the $\overline{\Gamma}\,\overline{X}$ direction are only replicas from the specular $\Delta k_{\parallel} = 0$ spectra.

Finally, we discuss the specific line shape of the FK phonon and compare it with recent high-resolution optical data for a NiO(100) single crystal. As we have shown in Fig. 3, the spectral response in the region of the FK phonon polariton is independent of the specific electron energy. It follows approximately the dielectric surface-loss function

$$I(\omega) \sim \mathrm{Im}\left(\frac{\varepsilon(\omega)}{\varepsilon(\omega)+1}\right),$$

where $\varepsilon(\omega)$ is the complex dielectric function of bulk NiO. This relation holds if the phonon properties within the NiO film can be fully described by the NiO bulk properties and describes the surface-bound phonon polariton.[13,14] The complex bulk dielectric function is on the other hand experimentally accessible from high-resolution infrared reflectivity measurements and a Kramers-Kronig analysis via

$$R(\omega) = \left|\frac{\sqrt{\varepsilon(\omega)}-1}{\sqrt{\varepsilon(\omega)}+1}\right|^2.$$

To retrieve the surface-loss function, the bulk reflectivity data of Kant *et al.*,[7] as shown by open symbols in Fig. 9(a), have been modeled with a generalized oscillator model. The model (solid red line) describes the experiment well and is described by a high-frequency permittivity $\varepsilon_{\infty} = 5.25$ and two independent transversal optical eigenfrequencies at 399 and 563 cm^{-1} with damping terms of 13.8 and 68 cm^{-1}. This generalized oscillator model is frequently used to describe the dielectric response in the phonon region of transition metal oxides. With very similar fitting parameters of two oscillators, it has been applied earlier to the NiO bulk properties in the work of Gielisse *et al.* and Mochizuki *et al.*[35,36] Note that a description based on a single damped oscillator, as shown by the dashed blue line in Fig. 9(a), fails to describe the details of the reflectivity. Especially, the steplike behavior in the reflectivity at about 560 cm^{-1} requires a second oscillator, which corresponds to a splitting of the optical modes.

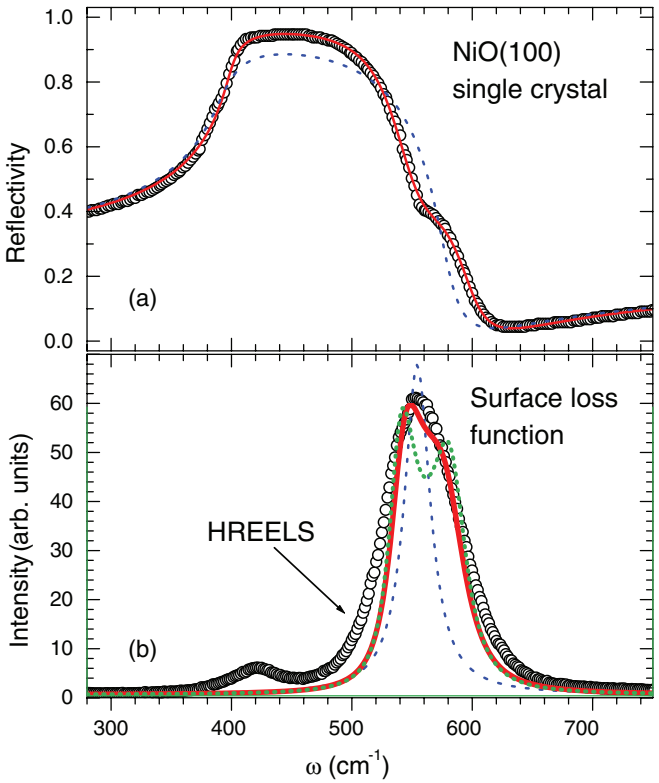

FIG. 9. (Color online) (a) Experimental NiO bulk-reflectivity data as adopted from Ref. 7 (solid symbols) and calculated reflectivity based on a generalized oscillator model with two (red solid line) and one oscillator (blue dashed line). (b) HREELS data (open circles) in the region of the FK phonon and calculated surface-loss function as derived from the bulk modeling in (a) (solid red and blue dashed lines). Additionally the surface-loss function with a reduced damping (see text) is displayed as green dotted line.

Whereas the zone-center splitting of the TO phonons of the transition metal monoxide has been successfully described in terms of an antiferromagnetically induced or exchange-driven splitting,[8,9,37] earlier work refers the LO-phonon splitting also to a combinational mode of Brillouin zone boundary acoustic and optical phonons,[35] anharmonicity effects in the lattice potential or to the deformation of the ionic-charge distribution during lattice vibration.[36]

In Fig. 9(b), the electron energy-loss spectrum is displayed in the region of the FK phonon together with the calculated surface-loss function (solid red line). The surface-loss function has been derived from the complex bulk dielectric function, which is based on the two-oscillator model and which describes the bulk reflectivity data perfectly. For comparison, the surface-loss function for the single oscillator model is shown as a dashed blue line. In the latter case, the loss function corresponds to a narrow Lorentzian-like peak where the peak position is in agreement with the experimental data. However, the narrow peak width cannot account for the experimental data. On the other hand, the optical bulk data predict a splitting of the FK phonon mode, which can be traced back to the steplike reflectivity change at about 560 cm^{-1}. Only by modeling this steplike reflectivity properly are we able to describe the broad experimental lineshape of the FK phonon. To emphasize this new FK phonon splitting further, the surface-loss function has been also calculated for a reduced second phonon damping constant (from 68 to 50 cm^{-1}) but with otherwise unchanged parameters. It is plotted in Fig. 9(b) as a green dotted line for comparison and results in two 50 cm^{-1} separated maxima as can be clearly seen. This comparison shows directly that the FK splitting due to the bulk optical phonon splitting accounts for the experimental FK lineshape.

IV. CONCLUSIONS

The surface-phonon dispersion of a 25-ML-thick NiO(100) layer on Ag(100) has been studied by HREELS along the high-symmetry $\overline{\Gamma}\,\overline{X}$ direction and compared with theoretical data. The epitaxial layer that has been grown at room temperature is well-ordered, as evidenced by monitoring the elastic peak intensity between the centers of two neighboring SBZ along $\overline{\Gamma}\,\overline{X}\,\overline{\Gamma}'$ direction. Along the $\overline{\Gamma}\,\overline{X}$ direction of the SBZ, six different surface phonons have been identified by analysis of spectra recorded under different scattering geometries and with primary electron kinetic energies between 4 and 196 eV. All surface-phonon dispersion data are compared with DFT + U calculations of the surface-projected bulk phonon bands to address spectral regions in reciprocal space that allow true surface modes. The experimentally determined acoustic surface Rayleigh phonon (S_1) shows a strong upward dispersion up to 173 cm^{-1} at the $\overline{X}$ point, in good agreement with HAS data for a NiO(100) single crystal.[12] Its dispersion follows the bulk acoustic band edge. The Wallis (S_2) and the Lucas (S_4) surface phonons have been observed at 425 and 367 cm^{-1} at the $\overline{\Gamma}$ point, respectively. Both modes show only a weak downward dispersion from the $\overline{\Gamma}$ to the $\overline{X}$ point. At energies below the Lucas mode, the S_6 surface phonon is observed at the zone boundary, which turns into a surface resonance at the zone center. Additionally, a new phonon mode has been identified at the zone boundary at 194 cm^{-1}. In summary, besides the FK phonon, the dispersion of five additional surface-phonon modes has been determined and compared with the surface-projected bulk phonons. These data might stimulate more involved calculation of the surface phonons, which could then allow a deeper understanding of the character of the surface excitations and their coupling to bulk modes.

The FK phonon polariton, which is located at 559 cm^{-1} independent of the scattering condition, is the most intense energy loss at nearly all scattering conditions. Its dispersionless behavior is explained by a dominant dipole-scattering mechanism for this mode. The FK loss shows a specific non-Lorentzian lineshape, which is compatible with a surface phonon-polariton splitting resulting from the splitting of bulk optical phonons due to the antiferromagnetic order. Calculations of the surface-loss function via the complex dielectric function from literature data of the normal-incidence reflectivity of a NiO(100) single crystal support this proposition.

ACKNOWLEDGMENT

Support by the German joint research network Sonderforschungsbereich 762 “Functionality of oxidic interfaces” of the Deutsche Forschungsgemeinschaft is gratefully acknowledged.

*wolf.widdra@physik.uni-halle.de

[1] G. A. Sawatzky and J. W. Allen, Phys. Rev. Lett. **53**, 2339 (1984).
[2] S. Hüfner, P. Steiner, I. Sander, M. Neumann, and S. Witzel, Z. Phys. B **83**, 185 (1991).
[3] S. Hüfner, Adv. Phys. **43**, 183 (1994).
[4] W. Reichardt, V. Wagner, and W. Kress, J. Phys. C **8**, 3955 (1975).
[5] R. A. Coy, C. W. Tompson, and E. Gürmen, Solid State Commun. **18**, 845 (1976).
[6] W. D. Luo, P. H. Zhang, and M. L. Cohen, Solid State Commun. **142**, 504 (2007).
[7] C. Kant, F. Mayr, T. Rudolf, M. Schmidt, F. Schrettle, J. Deisenhofer, and A. Loidl, Eur. Phys. J.-Spec. Top. **180**, 43 (2010).
[8] A. Floris, S. de Gironcoli, E. K. U. Gross, and M. Cococcioni, Phys. Rev. B **84**, 161102 (2011).
[9] C. Kant, M. Schmidt, Z. Wang, F. Mayr, V. Tsurkan, J. Deisenhofer, and A. Loidl, Phys. Rev. Lett. **108**, 177203 (2012).
[10] C. Oshima, Mod. Phys. Lett. B **05**, 381 (1991).
[11] W. P. Brug, G. Chern, J. Duan, G. G. Bishop, S. A. Safron, and J. G. Skofronick, J. Vac. Sci. Technol. A **10**, 2222 (1992).
[12] G. Witte, P. Senet, and J. P. Toennies, Phys. Rev. B **58**, 13264 (1998).
[13] R. Fuchs and K. L. Kliewer, Phys. Rev. **140**, A2076 (1965).
[14] K. L. Kliewer and R. Fuchs, Phys. Rev. **144**, 495 (1966).
[15] P. A. Cox and A. A. Williams, Surf. Sci. **152–153**, 791 (1985).
[16] K. W. Wulser and M. A. Langell, Phys. Rev. B **48**, 9006 (1993).
[17] K. W. Wulser and M. A. Langell, Surf. Sci. **314**, 385 (1994).
[18] R. F. Wallis, D. L. Mills, and A. A. Maradudin, in *Localized Excitation in Solids*, edited by R. F. Wallis (Plenum, New York, 1968), p. 403.
[19] A. A. Lucas, J. Chem. Phys. **48**, 3156 (1968).
[20] J. P. Toennies, G. Witte, A. M. Shikin, and K. H. Rieder, J. Electron Spectrosc. Relat. Phenom. **64-66**, 677 (1993).
[21] K. L. Kostov, S. Polzin, and W. Widdra, J. Phys.: Condens. Matter **23**, 484006 (2011).
[22] K. L. Kostov, M. Gzell, P. Jakob, T. Moritz, W. Widdra, and D. Menzel, Surf. Sci. **394**, L138 (1997).
[23] K. L. Kostov, D. Menzel, and W. Widdra, Phys. Rev. B **61**, 16911 (2000).
[24] K. L. Kostov, W. Widdra, and D. Menzel, J. Phys. Chem. B **108**, 14324 (2004).
[25] R. Heid, K.-P. Bohnen, T. Moritz, K. L. Kostov, D. Menzel, and W. Widdra, Phys. Rev. B **66**, 161406 (2002).
[26] K. Marre and H. Neddermeyer, Surf. Sci. **287-288**, 995 (1993).
[27] K. Marre, H. Neddermeyer, A. Chasse, P. Rennert, Surf. Sci. **357–358**, 233 (1996).
[28] P. A. Thiry, M. Liehr, J. J. Pireaux, and R. Caudano, Phys. Rev. B **29**, 4824 (1984).
[29] J. L. Guyaux, P. Lambin, and P. A. Thiry, Prog. Surf. Sci. **74**, 319 (2003).
[30] G. Dalmai-Imelik, J. C. Bertolini, and J. Rousseau, Surf. Sci. **63**, 67 (1977).
[31] G. T. Tyuliev and K. L. Kostov, Phys. Rev. B **60**, 2900 (1999).
[32] S. Sachert, S. Polzin, K. L. Kostov, and W. Widdra, Phys. Rev. B **81**, 195424 (2010).
[33] M.-L. Xu, B. M. Hall, S. Y. Tong, M. Rocca, H. Ibach, S. Lehwald, and J. E. Black, Phys. Rev. Lett. **54**, 1171 (1985).
[34] H. Ibach and D. L. Mills, *Electron Energy Loss Spectroscopy and Surface Vibrations* (Academic Press, New York, 1982).
[35] P. J. Gielisse, J. N. Plendl, L. C. Mansur, R. Marshall, S. S. Mitra, R. Mykolaje, and A. Smakula, J. Appl. Phys. **36**, 2446 (1965).
[36] S. Mochizuki and M. Satoh, Phys. Status Solidi B **106**, 667 (1981).
[37] S. Massidda, M. Posternak, A. Baldereschi, and R. Resta, Phys. Rev. Lett. **82**, 430 (1999).